Applied Physics B (2018) 124:148
https://doi.org/10.1007/s00340-018-7018-6

Applied Physics B
Lasers and Optics

Multiwavelength differential absorption lidar to improve measurement accuracy: test with ammonia over a traffic area

Riccardo Rossi[1] · Jean-François Ciparisse[1] · Andrea Malizia[2] · Michela Gelfusa[1] · Pasquale Gaudio[1]

Received: 20 March 2018 / Accepted: 23 June 2018 / Published online: 27 June 2018

Abstract
The development and improvement of techniques to monitor off-normal concentrations of chemicals in the atmosphere are crucial to guarantee human and environmental health, safety, and security. An interesting technique for use in research activities is the differential absorption lidar (DIAL); an improvement of the lidar technique able to provide information about the concentration of chemicals in the atmosphere. This work is focused on the use of DIAL, using a multiwavelength approach to increase the accuracy of gas concentration measurements in the atmosphere. The authors perform the uncertainty propagation analysis of this method, and highlight the advantages and the limits of this technique. Then, they applied this multiwavelength technique to preliminary DIAL measurements of ammonia in the atmosphere using three couples of laser wavelengths. The measurements are performed over a traffic area and are compared with water vapour measurements. A strong correlation between ammonia and water has been found a symptom that both chemicals belong to the exhaust gases of vehicles.

1 Introduction

The continuous monitoring of the atmosphere is a key factor to prevent human diseases and environmental disasters. The pollution due to human activities led to an increase in global warming, and the effect of pollution on human health is proved and clear [1–4]. Several diseases are strictly correlated to the effect of pollution, such as lung diseases, Leukaemia (benzene vapours), birth defects, and cardiovascular problems, and the incidence of these diseases usually increases in industrialised places [5–8]. Moreover, air pollution is not the only risk related to chemicals in the atmosphere. Accidental releases of hazardous chemicals threat all the industries that work with dangerous agents. Some chemicals normally used in the industries could be fatal for humans if breathed in large quantities [9–11]. Consider the accident in Bangladesh happened the 23 August 2016, where there was an accidental release of ammonia and 25 people had fallen in. Furthermore, deliberate chemical releases should be also considered. Hazardous chemicals may be released with the intention to cause injuries, deaths, and panic in a hostile population [11, 12]. Therefore, the role of monitoring is clear: detect and identify off-normal concentrations of chemicals that may cause environmental and health issues to respond properly to unconventional events [13–15].

Among the several measurement techniques of chemicals in the atmosphere, the areal remote sensing applications are attractive because of their property to measure large area by means of only one measurement station. An interesting technique able to detect, identify, and quantify the concentration is the differential absorption LIDAR (DIAL), which is an evolution of the light detection and ranging (LIDAR) technique [16, 17]. The LIDAR is applied in different fields, such as agriculture, biology, meteorology, and military applications [18–23]. In the field of environmental monitoring, LIDAR has been used to detect fires in outdoor environments [24, 25], exploiting different optical properties of smoke with the air. The technique is based on the measurement of the backscattered light emitted by a laser. This light is a function of the optical properties of the medium crossed by the laser light. However, the LIDAR is able to detect some variations in the atmosphere, based on the extinction coefficient, but is not able to identify and quantify it [16, 17, 26]. Sometimes, it is possible, under specific hypotheses, to

✉ Riccardo Rossi
R.Rossi@ing.uniroma2.it; Riccardo.Rossi.en@gmail.com

[1] Department of Industrial Engineering, The University of Rome "Tor Vergata", Via del Politecnico 1, 00133 Rome, Italy

[2] Department of Biomedicine and Prevention, The University of Rome "Tor Vergata", Via del Politecnico 1, 00133 Rome, Italy

measure the molecular and particulate backscattering [27]. This limit is overtaken by the DIAL technique that uses two different wavelengths with which it gives the concentration of the measured chemical [28–30]. Important advantages of the DIAL technique are the high sensitivity per laser probe energy, the variety of measurable chemicals, and the higher degree of eye safety if far infrared lasers are used [31]. Several studies confirm the capability to use the DIAL technique to monitor the atmosphere. Robinson et al. [32, 33] used an infrared DIAL to measure the hydrocarbon emissions from petrochemical and landfill installations. The same techniques allowed to Rina Sa et al. [28] the measurements of sulfur dioxide, nitrogen dioxide, and nitric dioxide. Water vapour, ozone, and carbon dioxide have been measured by means of DIAL in several works [30, 34–36] during the last years.

The monitoring of ammonia is an important issue in both environmental and safety fields. The increase of ammonia in the atmosphere is strictly correlated to eutrophication and acidification of ecosystems [37, 38]. It also plays a crucial role in the formation of secondary particulate matter because of interaction with acidic species [39, 40]. Ammonia emissions belong to agriculture activities, industries, and vehicles [41–43]. Furthermore, ammonia is a toxic gas. The Occupational Safety and Health Administration (OSHA) has set a 15-min exposure limit for gaseous ammonia of 35 ppm, while the 8-h exposure limit is 25 ppm. High exposure to ammonia can lead to lung damages and death [43, 44].

The DIAL technique is a sensitive method that requires a deep attention to have an accurate measurement. In fact, this technique is deeply influenced by each noise source in the atmosphere and this problem is usually overtaken by means of simplified hypotheses. Most of them may involve a systematic error in the DIAL measurement. In this work, the authors provide a description of some of these noises. An innovative approach to increase the accuracy of DIAL technique has been developed by Xiang et al. [45]. They suggest the use of more "off" wavelengths to minimize the uncertainty of DIAL measurements. In the present work, the authors propose a generalization and variation of this multiwavelength approach, discussing the use of more "on" and "off" line pairs, to maximize the accuracy of the method. This work analyses how the systematic error due to differential extinction coefficients and backscattered coefficients varies when this approach is adopted. This method is applied to the measurement of ammonia in the atmosphere, over a large traffic area.

Section 2 presents the performance of our system to make measurements of several chemicals compounds changing the laser wavelength. It discusses how data are analysed, the uncertainty analysis, and system sensitivity, and it shows the generalization of multiwavelength approach. Section 3 reports the concentration of temporal map of ammonia and water diffusion obtained through the measurements campaign. To evaluate the goodness of ammonia measurements, the authors also measured the water vapour concentration at the same times and in the same area. In fact, ammonia and water should have a positive correlation in traffic areas (if water increase, ammonia increases), since water is a combustion product and ammonia is used in selective catalytic reduction (SCR). The correlation between ammonia and water will be shown. The results show a proper capability of the system to monitor ammonia concentration in large areas. The DIAL system associated with the multiwavelength approach is able to measure low ammonia concentrations (< 0.1 ppm). It ensures a good capability of the system to provide a proper and fast response in case of off-normal ammonia values in the environment.

2 Materials and methods

This section describes the experimental apparatus developed to perform DIAL measurements. Then, it discusses the signal processing and the multiwavelength approach, the technique introduced by Xiang et al. [45].

2.1 Experimental apparatus

The authors developed an experimental apparatus able to perform measurement of chemical compounds in the atmosphere. The system used works into infrared windows (9–11 μm) corresponding to CO_2 laser emission. The system is based on DIAL technologies.

Figure 1 shows a schematic layout and a photo of the experimental apparatus. The transmitter is based on the CO_2 laser (MTL-5 mini TEA CO_2). It has 50 ns laser pulse width, a maximum repetition rate of 200 Hz. A manual grating, mounted into the laser cavity, allows an

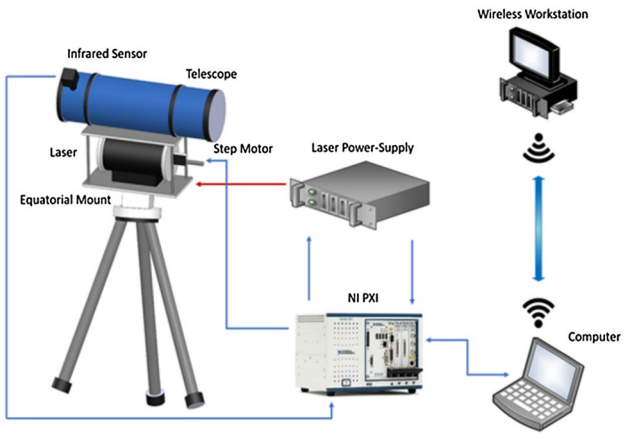

Fig. 1 Schematic representation of the main components of the experimental apparatus

output radiation between more than 60 lines. The maximum energy is 50 mJ per pulse at 10P20 laser line. The grating is tuned by means of a step motor (Mercury™ II DC-Motor Controller/Driver) controlled via software that allows an automatization of the laser tuning. The backscattered signal is collected by the Newtonian telescope (model Ziel GALAXY 2). It is provided with a primary mirror of the diameter of 200 mm and a focal length of 1000 mm. The backscattered signal is focalised into the infrared sensor (liquid nitrogen cooled MCT infrared detectors). It converts the backscattered signal into an electrical one, digitalised by a Data Acquisition (DAQ) system National Instrument PXI standard. The PXI is provided with three NI cards: NI PXI-6509, NI PXI-5122, and NI PXI-7330. The card NI PXI-6509 is an industrial digital I/O that is used to send a trigger signal to the laser power supply. The card NI PXI-5122 is a 14-bit 100 MS/s Digitizer and it is used to acquire the data at 100 MHz. The card NI PXI-7330 is used to control the equatorial mount, which allows the orientation of the laser beam to perform areal measurements. The acquired data are stored and downloaded iteratively on a pc, which sends the data to a workstation through a wireless connection.

Figure 2 shows the main steps done by the PXI and the workstation. The PXI and the workstation work separately. The PXI is able to control and acquire the backscattered signals, while the workstation is used to store concentration data of each chemical to analyse. The PXI functioning can be resumed as follows:

1. The step motor tunes the laser grating to the proper line.
2. The PXI sends a trigger signal (card NI PXI-6509) to enable the laser that sends a second trigger in order to synchronize the acquisition system (card NI PXI-5122) with every laser pulse. The card NI PXI-5122 acquires the backscattered signal. This step is repeated N times, where N is the number of pulses per line that users desire.
3. When all the backscattered signals for every laser line chose are acquired, the system starts with a new scan.

The workstation is provided by a routine able to calculate the concentration by means of DIAL equation. The number of pulse per laser line is 100 and the repetition rate is 10 Hz. The software for the device control, data acquisition, and analysis are written in LabVIEW.

The measurements shown in the present paper are performed in an urban area near the University of Rome Tor Vergata. The laser beam is sent over a roundabout, where vehicular traffic is very high. The measurements have been effectuated on a typical autumn day from 11:00 to 16:30. A measurement break has been done due to the lunch break, i.e., from 1 am to 2 am (13:00 to 14:00). Figure 3 shows the map area crosses by the laser beam where it is possible identified four different zones. In the first and second regions, from 0 to 100 and from 100 to 175 m, the laser beam crosses a parking area where the traffic usually is very low, except at the beginning and at the end of the working time. Therefore, pollution is expected from 10:45 to 11:30 am, from 1 to 2 pm (lunchtime), and between 15:45 to 16:30. In the third region, from 175 m to about 300 m, the laser beam crosses the roundabout, which has usually high traffic at every hour

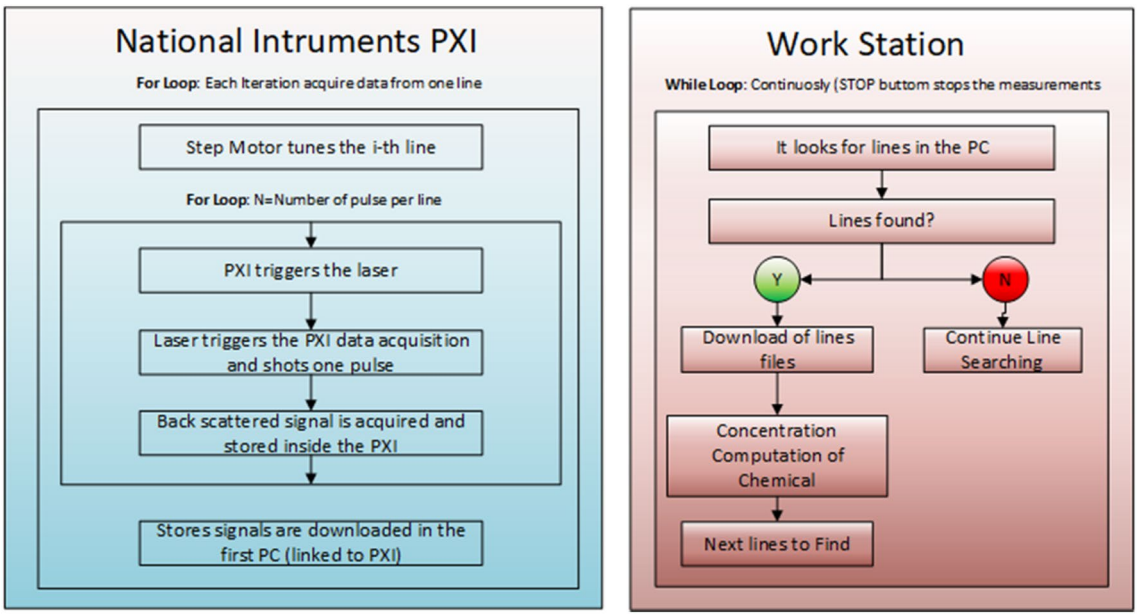

Fig. 2 Flowchart of the functioning of the DIAL system. It shows the main steps done by the PXI and the workstation

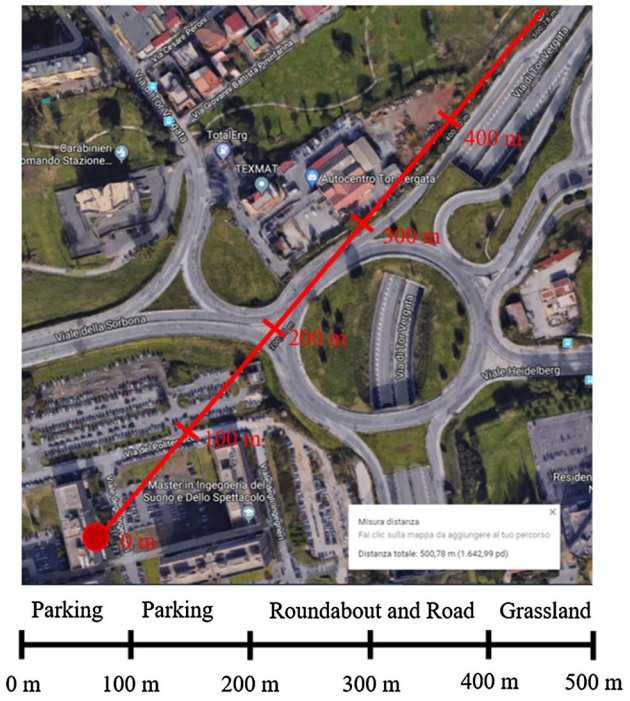

Fig. 3 Map representing the direction of measurements and the various distance

of the day. In the last region, over 300 m, the laser beam crosses a grassland.

2.2 Signal analysis

The differential absorption lidar (DIAL) exploits the shape of absorption spectra of chemicals to perform quantitative measurements [17]. An absorption spectrum is characterized by several peaks at different wavelengths. The density equation by the DIAL measurement is as follows:

$$N(R) = \frac{1}{2\,\Delta\sigma}\left\{\frac{\mathrm{d}}{\mathrm{d}R}\left[\ln\left(\frac{P_{\mathrm{off}}(R}{P_{\mathrm{on}}(R}\right) - \ln\left(\frac{\beta_{\pi,\mathrm{off}}(R}{\beta_{\pi,\mathrm{on}}(R}\right)\right] + k_{\mathrm{off}}(R - k_{\mathrm{on}}(R\right\}, \tag{1}$$

where $N(R)$ is the concentration of the chemical compound versus distance (R), $\Delta\sigma$ is the differential absorption cross section, defined as σ_{on} minus σ_{off}; where σ_{on} is the absorption cross section of laser wavelength strongly absorbed, and σ_{off} is the absorption coefficient of laser wavelength not strongly absorbed. P_{off} and P_{on} are, respectively, the power backscattered signal in the two cases. $\beta_{\pi,\mathrm{off}}$ and $\beta_{\pi,\mathrm{on}}$ are the backscattering coefficients, and k_{off} and k_{on} are the extinction coefficients at the two wavelengths.

The influence of backscattering and extinction coefficients is usually neglected, and a simplified equation is achieved:

$$N(R) = \frac{1}{2\,\Delta\sigma}\left\{\frac{\mathrm{d}}{\mathrm{d}R}\left[\ln\left(\frac{P_{\mathrm{off}}(R)}{P_{\mathrm{on}}(R)}\right)\right]\right\}. \tag{2}$$

In this work, the backscattered signals are calculated as the average of 100 signals. The software routine also computes the standard deviation, which is used for the uncertainty analysis. A symmetric moving average filter is also applied to the backscattered signals to smooth the high-frequency oscillations, due to random noise and atmospheric turbulence. The background is removed from each signal. It is measured how the detector signals in the absence of the laser beam. The backscattered signal ratio is calculated, and another moving average filter is applied. The rank of both moving average filters is 10. The use of these filters involves a decrease of the spatial resolution, that is reasonable because of the pulse width of the laser beam [17]. The logarithm is applied and so the derivative operation. The derivative of the signal is done using a central finite-difference method.

The DIAL measurements are affected by a minimum detectable concentration, which is a function of the chemical compound measured, experimental apparatus characteristics, and range. Two different curves limit the minimum readable concentration. The first curve is a function of the minimum LIDAR return (ΔP), usually determined by the noise equivalent power (NEP) [46]:

$$N_{\min(R)} = \frac{\mathrm{NEP}\pi R}{2\xi\rho A P\Delta\sigma\exp(-2k_{\mathrm{off}}R)}, \tag{3}$$

where ξ is the detector efficiency, ρ is the reflectivity, A is the area of the receiving telescope, and k_{off} is the "off" atmosphere extinction coefficient. In our case, these parameters have been taken as follows: NEP = 2.2E–8W; ξ = 0,9; ρ = 0,1; A = 0,031 m^2; P = 1E6W. The extinction coefficient can be taken equal to 0.12 km^{-1} [46–48].

The other important limit is characterized by the minimum fractional change in the LIDAR return ($\Delta P/P_{\mathrm{off}}$) [46]:

$$N_{\min(R)} = \frac{(P_{\mathrm{off}} - P_{\mathrm{on}})/P_{\mathrm{off}}}{2\Delta\sigma R}. \tag{4}$$

Since the first is an increasing function, while the second curve has a decreasing trend, the minimum and maximum ranges are strictly limited by both.

The uncertainty of DIAL measurements can be estimated by different approaches. Here, the authors use the uncertainty propagation theory [16]:

$$\delta N = \frac{1}{2\Delta\sigma\Delta R}\sqrt{\left(\frac{\delta P_{\text{on}}(R)}{P_{\text{on}}(R)}\right)^2 + \left(\frac{\delta P_{\text{on}}(R+\Delta R)}{P_{\text{on}}(R+\Delta R)}\right)^2 + \left(\frac{\delta P_{\text{off}}(R)}{P_{\text{off}}(R)}\right)^2 + \left(\frac{\delta P_{\text{off}}(R+\Delta R)}{P_{\text{off}}(R+\Delta R)}\right)^2}, \tag{5}$$

where $\delta(A)$ represents the uncertainty of the general variable A.

If the simplified equation (Eq. 2) is used, correction terms should be applied. The extinction coefficient is due to absorption and scattering molecules and particulate. The total correction due to the scattering of molecules and particulates can be evaluated as follows:

$$\Delta N_{\text{scattering}}(R) = -B_\lambda[u\beta_{p,\text{off}}(R) + 4\beta_{p,\text{off}}(R)], \tag{6}$$

where $\beta_{p,\text{off}}$ and $\beta_{m,\text{off}}$ are the scattering coefficient of particulate and molecules at the "off" wavelength, u is the Angstrom coefficient, and B_λ is the spectrum factor, which is a function of the wavelength difference ($\Delta\lambda = \lambda_{\text{on}} - \lambda_{\text{off}}$) and the differential absorption cross section:

$$B_\lambda = \frac{1}{\lambda_{\text{off}}\left[\frac{\Delta\sigma}{\Delta\lambda}\right]}. \tag{7}$$

The molecular scattering coefficient in function of the distance is usually calculated assuming a standard profile of the chemicals, while the particulate scattering is calculated through a reference line (which may be the "off" line if the absorption coefficient is negligible).

The absorption correction is usually negligible if there is not a strong differential absorption cross section of other chemicals. Thus, the correction can be estimated as follows:

$$\Delta N_{\text{absorption}}(R) = -\frac{1}{\Delta\sigma}\sum N_i(R)\Delta\sigma_i, \tag{8}$$

where N_i and $\Delta\sigma_i$ are the concentration and the differential absorption cross section of the ith chemical in the atmosphere. Note that this correction requires the measurement or the assumption of the other chemical concentrations.

The backscattering correction term is a function of the gradient of the particulate extinction coefficient and it is found by taking the derivative of the backscatter ratio:

$$\Delta N_{\text{backscattering}}(R) = -\frac{1}{2\,\Delta\sigma\Delta R}\left[\ln\left(\frac{\beta_{\pi,\text{on}}(R)}{\beta_{\pi,\text{on}}(R+\Delta R)}\right) - \ln\left(\frac{\beta_{\pi,\text{off}}(R)}{\beta_{\pi,\text{off}}(R+\Delta R)}\right)\right]. \tag{9}$$

Since this term is a function of the gradient of the differential backscattering, this term plays an important role only when the hypothesis of the homogeneous atmosphere is not allowed. For example, this term should be used when the laser beam crosses a cloud or a smoke plume [16]. Therefore, in this work, this correction term is not considered.

Another source of uncertainty is the wavelength tuning precision. In this work, the wavelength tuning is achieved by a step motor with a maximum error of 10 μm, which corresponds to a wavelength error much lower than 1%. In a previous work, the absorption uncertainty due to the wavelength tuning error has been evaluated experimentally, and it was completely insignificant. Thus, in this work, this uncertainty source has been neglected.

2.3 Multiwavelength approach

Xiang et al. [45] discussed the multiwavelength approach asserting an increase in the DIAL accuracy. They applied the method to CO_2 measurements profiles, showing significant accuracy improvements. Their method is based on the use of one "on" wavelength and many "off" wavelengths.

At first, the method is generalised to the use of not only many "off" wavelength, but also use of many DIAL couples of laser lines. Therefore, consider m "on" and "off" DIAL couples and let us write a DIAL equation for each combination:

$$\begin{cases} N_1(R) = \frac{1}{2\,\Delta\sigma}\left\{\frac{\mathrm{d}}{\mathrm{d}R}\left[\ln\left(\frac{P_{\text{off},1}(R)}{P_{\text{on},1}(R)}\right)\right]\right\} \\ N_2(R) = \frac{1}{2\,\Delta\sigma}\left\{\frac{\mathrm{d}}{\mathrm{d}R}\left[\ln\left(\frac{P_{\text{off},2}(R)}{P_{\text{on},2}(R)}\right)\right]\right\} \\ \vdots \\ N_m(R) = \frac{1}{2\,\Delta\sigma}\left\{\frac{\mathrm{d}}{\mathrm{d}R}\left[\ln\left(\frac{P_{\text{off},m}(R)}{P_{\text{on},m}(R)}\right)\right]\right\} \end{cases}. \tag{10}$$

Through the least square method, they arrived at the final equation that computes the chemical concentration as the weighted average of the measurements, where the weight is the square of the differential absorption cross section:

$$N_{\text{final}}(R) = \sum_{i=1}^{m}\frac{\Delta\sigma_i^2}{\sum_{i=1}^{m}\Delta\sigma_i^2}N_i(R). \tag{11}$$

Different "on" and "off" lines could be used to smooth out systematic errors of single lines. On the other hand, the use of different couples, and not only the change of only the "off" line, makes sense only if the differential absorption cross sections have the same order of magnitude.

Therefore, the uncertainty of multiwavelength method can be estimated using again the uncertainty propagation theory:

$$\delta N_{\text{final}} = \frac{1}{\sum_{i=1}^{m} \Delta\sigma_i^2} \sqrt{\sum_{i=1}^{m} \left(\Delta\sigma_i^2 \delta N_i\right)^2}, \tag{12}$$

where δN represents the uncertainty of N variable. The uncertainties of differential absorption cross sections have been neglected. This equation highlights that multiwavelength approaches could have uncertainty larger and smaller than some DIAL couples. Therefore, the convenience of multiwavelength approach should be validated for each couple combination of laser lines. The authors want to underline that the multiwavelength method is based on the minimization of the least squares. It represents the best combination of couples and if there are a couple which worsens the uncertainty, they should be removed.

The multiwavelength DIAL equation showed before (Eq. 11) is computed using the approximated DIAL equation (Eq. 2), where the differential extinction coefficients and the backscattering coefficient influences are neglected. The complete multiwavelength DIAL equation can be achieved by Eq. 1. Then, the error can be calculated if the simplified equation is used. If the complete DIAL equation is considered, the system in Eq. 10 must be modified as follows:

$$\begin{cases} N_1(R) = \dfrac{1}{2\,\Delta\sigma_1}\left\{\dfrac{\mathrm{d}}{\mathrm{d}R}\left[\ln\left(\dfrac{P_{\text{off},1}(R)}{P_{\text{on},1}(R)}\right) - \ln\left(\dfrac{\beta_{\text{off},1}(R)}{\beta_{\text{on},1}(R)}\right)\right] + k_{\text{off},1}(R) - k_{\text{on},1}(R)\right\} \\ N_2(R) = \dfrac{1}{2\,\Delta\sigma_2}\left\{\dfrac{\mathrm{d}}{\mathrm{d}R}\left[\ln\left(\dfrac{P_{\text{off},2}(R)}{P_{\text{on},2}(R)}\right) - \ln\left(\dfrac{\beta_{\text{off},2}(R)}{\beta_{\text{on},2}(R)}\right)\right] + k_{\text{off},2}(R) - k_{\text{on},2}(R)\right\} \\ N_2(R) = \dfrac{1}{2\,\Delta\sigma_2}\left\{\dfrac{\mathrm{d}}{\mathrm{d}R}\left[\ln\left(\dfrac{P_{\text{off},2}(R)}{P_{\text{on},2}(R)}\right) - \ln\left(\dfrac{\beta_{\text{off},2}(R)}{\beta_{\text{on},2}(R)}\right)\right] + k_{\text{off},2}(R) - k_{\text{on},2}(R)\right\} \end{cases}. \tag{13}$$

Introduce the error ε and let us write the system as follows:

$$\begin{cases} 2\,\Delta\sigma_1 N_1(R) = \dfrac{\mathrm{d}}{\mathrm{d}R}\left[\ln\left(\dfrac{P_{\text{off},1}(R)}{P_{\text{on},1}(R)}\right) - \ln\left(\dfrac{\beta_{\text{off},1}(R)}{\beta_{\text{on},1}(R)}\right)\right] + k_{\text{off},1}(R) - k_{\text{on},1}(R) + \varepsilon_1 \\ 2\,\Delta\sigma_2 N_2(R) = \dfrac{\mathrm{d}}{\mathrm{d}R}\left[\ln\left(\dfrac{P_{\text{off},2}(R)}{P_{\text{on},2}(R)}\right) - \ln\left(\dfrac{\beta_{\text{off},2}(R)}{\beta_{\text{on},2}(R)}\right)\right] + k_{\text{off},2}(R) - k_{\text{on},2}(R) + \varepsilon_2 \\ 2\,\Delta\sigma_n N_n(R) = \dfrac{\mathrm{d}}{\mathrm{d}R}\left[\ln\left(\dfrac{P_{\text{off},n}(R)}{P_{\text{on},n}(R)}\right) - \ln\left(\dfrac{\beta_{\text{off},n}(R)}{\beta_{\text{on},n}(R)}\right)\right] + k_{\text{off},n}(R) - k_{\text{on},n}(R) + \varepsilon_n \end{cases}. \tag{14}$$

Let us call:

$$\boldsymbol{B} = \begin{bmatrix} 2\,\Delta\sigma_1 \\ 2\,\Delta\sigma_2 \\ \vdots \\ 2\,\Delta\sigma_n \end{bmatrix}, \quad \boldsymbol{L} = \begin{bmatrix} \dfrac{\mathrm{d}}{\mathrm{d}R}\left[\ln\left(\dfrac{P_{\text{off},1}(R)}{P_{\text{on},1}(R)}\right) - \ln\left(\dfrac{\beta_{\text{off},1}(R)}{\beta_{\text{on},1}(R)}\right)\right] + k_{\text{off},1}(R) - k_{\text{on},1}(R) \\ \dfrac{\mathrm{d}}{\mathrm{d}R}\left[\ln\left(\dfrac{P_{\text{off},2}(R)}{P_{\text{on},2}(R)}\right) - \ln\left(\dfrac{\beta_{\text{off},2}(R)}{\beta_{\text{on},2}(R)}\right)\right] + k_{\text{off},2}(R) - k_{\text{on},2}(R) \\ \dfrac{\mathrm{d}}{\mathrm{d}R}\left[\ln\left(\dfrac{P_{\text{off},n}(R)}{P_{\text{on},n}(R)}\right) - \ln\left(\dfrac{\beta_{\text{off},n}(R)}{\beta_{\text{on},n}(R)}\right)\right] + k_{\text{off},n}(R) - k_{\text{on},n}(R) \end{bmatrix} \boldsymbol{V} = \begin{bmatrix} \varepsilon_1 \\ \varepsilon_2 \\ \vdots \\ \varepsilon_n \end{bmatrix}. \tag{15}$$

Then, it follows the same procedure of the Xiang et al.'s work [45], which consist in the minimization of the least squares (LSM). At first, Eq. 15 can be written in matrix form:

$$\boldsymbol{B}\boldsymbol{N_c}(R) = \boldsymbol{L} + \boldsymbol{V}. \tag{16}$$

The least squares can be written as $\mathbf{V^T V}$. Then, their minimization implies that their derivative must be zero:

$$\frac{\partial(\boldsymbol{V^T V})}{\partial \bar{N}_C(R)} = 0 \rightarrow 2\frac{\partial(\boldsymbol{V^T})}{\partial \bar{N}_C(R)}\boldsymbol{V} = 2\boldsymbol{B^T}(\boldsymbol{B}\boldsymbol{N_C}(R) - \boldsymbol{L}) = 0. \tag{17}$$

The resolution of the above equation leads to:

$$\boldsymbol{N_C}(R) = (\boldsymbol{B^T B})^{-1}\boldsymbol{B^T L}. \tag{18}$$

It represents the concentration measured by means of the complete DIAL equation. It can be written as follows:

$$N_c(R) = \frac{1}{\sum_{i=1}^{m} \Delta\sigma_i^2} \sum_{i=1}^{m} \Delta\sigma_i^2 \left\{ N_i - \frac{1}{2\,\Delta\sigma_i}\left[\frac{\mathrm{d}}{\mathrm{d}R}\left(\ln\left(\frac{\beta_{\text{off},i}(R)}{\beta_{\text{on},i}(R)}\right)\right) + k_{\text{off},i}(R) - k_{\text{on},i}(R)\right]\right\}. \tag{19}$$

Then, the error committed using the simplified equation is computed in this way:

$$\text{Error}\,(R) = N_c(R) - N_s(R) = \frac{1}{\sum_{i=1}^{m} \Delta\sigma_i^2} \sum_{i=1}^{m} \left\{ -\frac{\Delta\sigma_i}{2} \left[\frac{\mathrm{d}}{\mathrm{d}R} \left(\ln \left(\frac{\beta_{off,i}(R)}{\beta_{on,i}(R)} \right) \right) + k_{off,i}(R) - k_{on,i}(R) \right] \right\}. \tag{20}$$

This result shows that also the systematic error due to the single couple may be strongly decreased when the multiwavelength approach is used. Furthermore, systematic error with opposite signs decreases the global error. Thus, if all the couples are affected by the systematic errors with the same signs, the error does not change in significant ways.

The last term of Eq. 20 is the differential extinction coefficient (Δk), which is a function of the molecular and particulate scattering and absorption. Then, it follows:

$$\Delta k = k_{\text{on}} - k_{\text{off}} \propto \sum_{k=1}^{L-1} \sigma_{\text{on},k} N_k - \sum_{k=1}^{L-1} \sigma_{\text{off},k} N_k = \sum_{k=1}^{L-1} \Delta\sigma_k N_k,$$

where L is the number of each chemical in the atmosphere, and $L-1$ represents all the chemicals excluded the analysed one. This dependence is considered in the estimation of error in the section result.

3 Results and discussion

3.1 Analytical study

Here, the authors discuss the conditions that rend a multiwavelength approach advantageous.

The authors performed an analytical study using the uncertainty propagation equation (Eq. 12) and they show that large uncertainties may involve a final uncertainty larger than the most accurate couple, as it is shown in Fig. 4. In the first figure (a), the authors suppose to use only two couples. The characteristics (uncertainty and differential absorption cross section) of couple 2 are fixed. Its absorption cross section is 10 m^{-1} atm^{-1} and its uncertainty is 0.1 ppm. The values of the first couple vary. The three lines in the image represent the output uncertainties of the multiwavelength approach versus the uncertainty of the first line. Each graph line is obtained by varying the absorption cross section of the first couple (10, 20, and 30 m^{-1} ppm^{-1}). The green area represents where the multiwavelength approach is convenient in this case. Note that larger is the cross section of the "bad" couple and larger is the uncertainty of the multiwavelength profile.

The figure (b) shows the same parameter but using three couples, where the couple 2 and 3 have equal fixed uncertainties and cross sections. Their relative uncertainties are equal to 0.1 ppm, while three values are analysed for the differential absorption cross sections: 10, 20, and 30 m^{-1} ppm^{-1}. The figure shows that the output uncertainty decreases, and it is less influenced by the "bad" couple. Thus, there still exist values where the output uncertainty may be larger than 0.1 ppm.

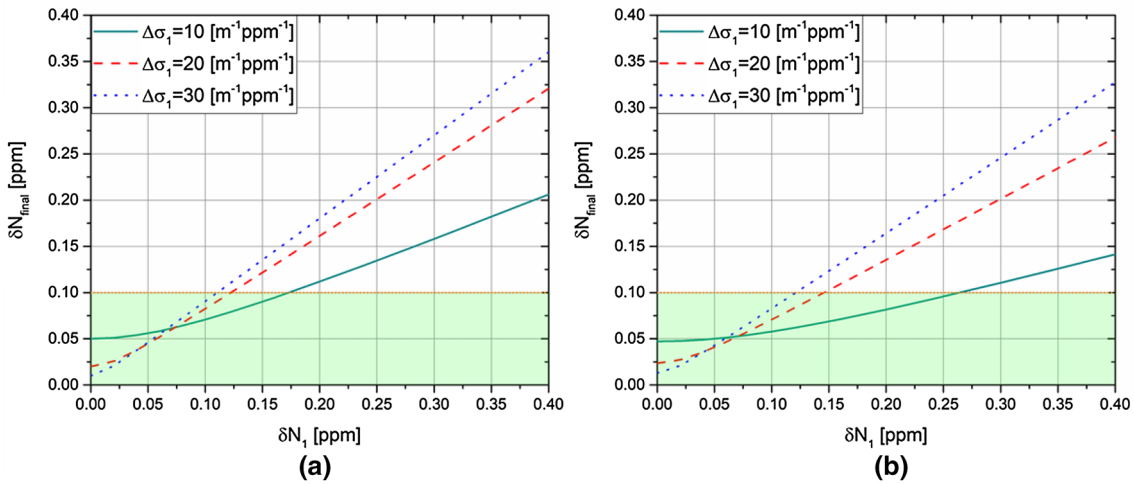

Fig. 4 Multiwavelength uncertainty in a function of couple uncertainties and cross-sections. The graph on the left (**a**) is achieved using only two couples, while the other graph (**b**) uses three couples. Graph **a** has one couple with a fixed cross section, equal to 10 ppm, and fixed uncertainty, equal to 0.1 ppm. The other couple cross section and uncertainty vary as described in the figure. **b** Two fixed couple with the same values of the graph (**a**). The green region shows the area where the multiwavelength approach involves an increase of the accuracy compared to the fixed couple uncertainty

The previous analysis has been done neglecting the total measurement time. However, it is an important parameter to consider when the two measurements are compared. Neglecting the line switching time, the single and the multiwavelength DIAL approaches have the same measurement time when each measurement performs the same number of laser shots. Suppose to use a number n of shots to perform the one-pair DIAL measurement (one pair of lines). If a multiwavelength approach with two pairs of lines is used, the number of shots per pair must be $n/2$. Thus, the final uncertainty of the one-pair DIAL will be:

$$\delta N_{\text{final, 1pair}} = \frac{\delta N_1}{\sqrt{n}}, \tag{21}$$

where δN_1 is the expected uncertainty of one measurement. In case of a multiwavelength approach where two pairs are used, Eq. 12 becomes:

$$\begin{aligned}\delta N_{\text{final,MW}} &= \frac{1}{\Delta\sigma_1^2 + \Delta\sigma_2^2}\sqrt{\frac{\Delta\sigma_1^2\delta N_1^2}{\frac{n}{2}} + \frac{\Delta\sigma_2^2\delta N_2^2}{\frac{n}{2}}} \\ &= \frac{1}{\Delta\sigma_1^2 + \Delta\sigma_2^2}\sqrt{\frac{2}{n}}\sqrt{\Delta\sigma_1^2\delta N_1^2 + \Delta\sigma_2^2\delta N_2^2}.\end{aligned} \tag{22}$$

In general, calling m the number of pairs used in the multiwavelength approach, the general uncertainty equation becomes:

$$\delta N_{\text{final,MW}} = \frac{1}{\sum_{i=1}^{m}\Delta\sigma_i^2}\sqrt{\frac{m}{n}}\sqrt{\sum_{i=1}^{m}\left(\Delta\sigma_i^2\delta N_i\right)^2}. \tag{23}$$

Thus, an efficiency factor of the multiwavelength approach can be obtained as follows:

$$\eta = \frac{\delta N_{\text{final, 1pair}}}{\delta N_{\text{final,MW}}} = \frac{\sum_{i=1}^{m}\Delta\sigma_i^2}{\sqrt{m}}\frac{\delta N_1}{\sqrt{\sum_{i=1}^{m}\left(\Delta\sigma_i^2\delta N_i\right)^2}}.$$

When η is larger than 1, it means that the multiwavelength approach leads to a smaller uncertainty of the one-pair DIAL.

Considering an analogous case to the previous one but taking into account that the measurements are limited by the same measurement time, and thus, the same number of lines, it is possible to provide similar graphs to Fig. 4. The results are the same of the previous case, where the only difference is that each multiwavelength uncertainty line is increased by a factor equal to $\sqrt{m}$, as shown in Fig. 5.

3.2 Chemicals analysed

To test the multiwavelength approach proposed, the concentration of water vapour and ammonia was made. Since the authors did not have other ammonia measurement devices, they chose to use the water vapour to validate the proposed technique and to compare the water vapour trends with ammonia, since a strong correlation is expected in a high traffic area. In fact, a good correlation between water vapour and ammonia values was expected, since the largest source of them is exhaust gases from vehicles. The measurements of water vapour are performed through a single couple

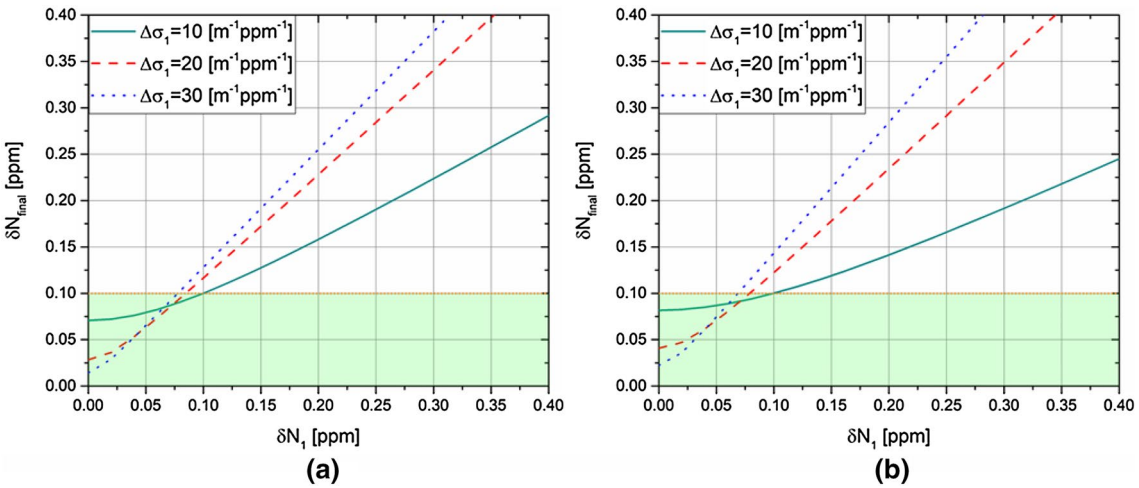

Fig. 5 Multiwavelength uncertainty in a function of couple uncertainties and cross sections, considering the same total averaging time. The graph on the left **a** is achieved using only two couples, while the other graph **b** uses three couples. Graph **a** has one couple with a fixed cross-section, equal to 10 ppm, and fixed uncertainty, equal to 0.1 ppm. The other couple cross section and uncertainty vary as described in the figure. **b** Two fixed couple with the same values of the graph (**a**). The green region shows the area where the multiwavelength approach involves an increase of the accuracy compared to the fixed couple uncertainty

wavelength approach. The laser lines chosen are the 10R20 (10.246625 μm) and 10R18 (10.260381 μm). The differential absorption cross section is 7.7 10^{-2} [m^{-1} atm^{-1}] [49, 50]. The use of other lines is meaningless for water vapour, since the other couples have a differential absorption cross section much smaller than the 10R20–10R18. The measurements of ammonia are performed with three different couples: 9R30 (on) and 9R28 (off), 9R08 (on) and 9R10 (off), and 10R08 (on) and 10R10 (off) [49–52]. The respectively differential absorption cross sections are listed in Table 1.

The correction terms to apply to the measured concentrations have been also estimated. In fact, the presence of other chemical compounds could affect the DIAL measurements when the value of the differential extinction coefficient due to them is not negligible. The correction term is calculated evaluating the differential extinction coefficient, equal to the product of the differential absorption cross section and the concentration. The correction due to absorption of molecules is negligible for any chemicals, excluded water vapour. In fact, the concentration of water vapour (see Sect. 3.3) is enough large to need correction.

Table 1 shows the estimation of water influence in each couple. The estimation of water is made assuming an average concentration of water equal to 15,000 ppm. The

Table 1 Differential absorption cross sections for each line couple

Line On	Line Off	$\Delta\sigma$ NH_3 (1/atm cm)	$\Delta\sigma$ H_2O (1/cm)	Delta K (ppm/cm)	Error (ppm)
9R30	9R28	55.98	1.434E−04	2.15E+00	3.84E−02
9R08	9R10	24.49	− 1.69E−05	− 2.54E−01	− 1.04E−02
10R08	10R10	22.13	2.518E−05	3.78E−01	1.71E−02
$\Sigma(\Delta\sigma\_NH_3)^2$ (1/cm^2)		4223.2574	Multiwavelength error (ppm)		2.90E−02

Evaluation of error due to the water presence. Positive errors imply an overestimation of the chemical measurement, while a negative error means an underestimation of the chemical compound

Table 2 Evaluation of molecular and particulate scattering influence in the DIAL measurements

	Water 10R20–10R18	Ammonia 9R8–9R10	Ammonia 9R30–9R28	Ammonia 10R8–10R10
λ on (μm)	10.24663	9.341758	9.21969	10.3337
λ off (μm)	10.26038	9.32937	9.22953	10.31842
$\Delta\sigma$ (1/m atm)	7.70E−02	2.55E+03	5.58E+03	2.55E+03
B_λ	0.017412	− 5.2E−07	1.91E−07	− 5.8E−07
Beta p (1/m)	1.20E-04	1.20E-04	1.20E-04	1.20E-04
Beta m (1/m)	1.20E-04	1.20E-04	1.20E-04	1.20E-04
$\Delta N_{scattering}$ (ppm)	-1.67E+01	5.00E-04	-1.83E-04	5.57E-04

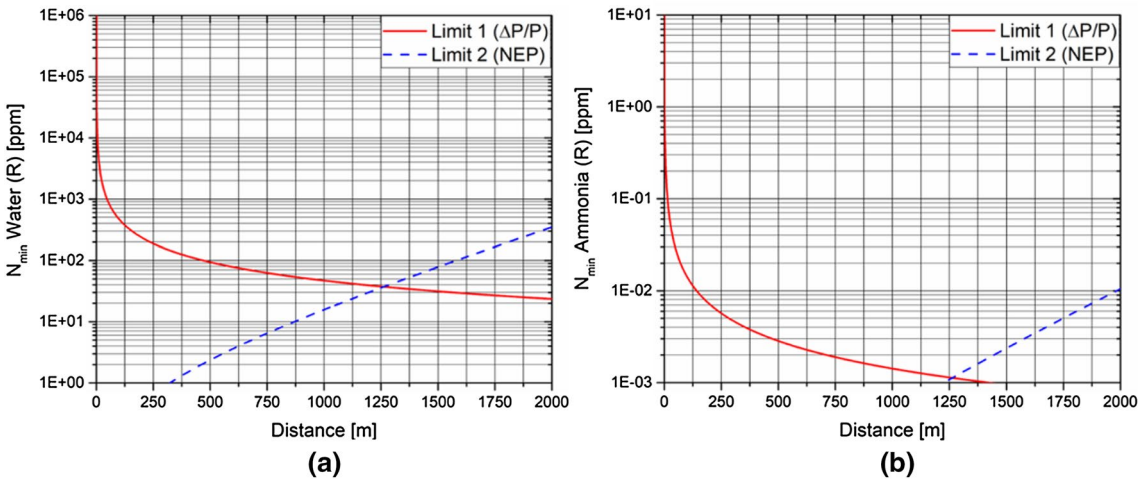

Fig. 6 Minimum readable concentration curves of water vapour and ammonia (10R08–10R10). The ammonia limit is calculated on the line with smaller differential absorption cross section (10R08–10R10), for a conservative value

most influenced couple by water vapour presence is the 9R30–9R28. The correction of water vapour on ammonia measurements is computed using the measured concentration profile. Table 1 also shows the error committed in case of multiwavelength approach if the correction is not applied (Eq. 18).

Table 2 shows the influence of particulate and molecule scattering in a worse case. The authors take a large value of Angstrom constant (4), and they overestimated both the scattering coefficients of molecules and particulate (0.12 km^{-1} is an appropriate value of the total extinction coefficient). Despite the overestimation, the influence of scattering coefficients is very low. Therefore, it is neglected in the measurements.

3.3 Minimum concentration curves and uncertainty analysis

At first, the graphs report the minimum readable concentration curves. Figure 6 shows the minimum concentration curves of water vapour (a) and ammonia (b). The lower distance limit has been chosen considering a minimum detectable water concentration equal to 1000 ppm that corresponds to a minimum distance of about 50 m. The maximum distance is determined not by the minimum concentration (the "NEP" curves is still low at 2 km) but by the limit curve equation hypothesis, which imposed that the product of minimum concentration, distance, and differential absorption cross section must be much lower than one (SNR) [46]. The authors decided for a maximum value of 1E-4 which corresponds to a maximum distance of 500 m (also, in this case, the minimum value is governed by water vapour). Therefore, the distance covers a range from 50 to 500 m. As illustrated in Fig. 3, the measurements line crosses a parking area (50–175 m), then the roundabout (175–300 m), and finally a green area (300–500 m).

Figure 7a shows the uncertainties profiles of water vapour and ammonia concentration in function of the distance *R*. The authors report only the uncertainty measured at 11:00 am for brevity; however, no significant differences have been observed with other measurements. Two important remarks could be done through this figure; first, the increase in uncertainty with the distance. Since the backscattered signals decrease with the distance, the relative uncertainty of the signal increases and it directly affects the concentration uncertainty (Eq. 4). This issue is another limit to the maximum range of the measurement. A second remark is about the hump of uncertainty trend between 200 and 300 m, that corresponds to the roundabout. In this case, the increase in uncertainty is due to the natural variability of the concentration. In fact, several vehicles cross this area during the measurement and it implies a high variable signal. Figure 7b compares the uncertainty of multiwavelength approach with the three couple of ammonia. The figure shows that the multiwavelength approach involves a significant decrease in uncertainty (25%), if compared with the most accurate couple (9R30–9R28). Then, the use of multiwavelength approach is proper in this case.

3.4 Water–ammonia measurements and their correlation

Figure 8 shows the results of the concentration of water vapour and ammonia in function versus range and time. Between the 12:30 am and the 14:00, there are not measurements available. On the day of measurement campaign, the maximum temperature in Rome was 27 °C, the minimum 12 °C, and the mean was 22 °C. Maximum humidity was

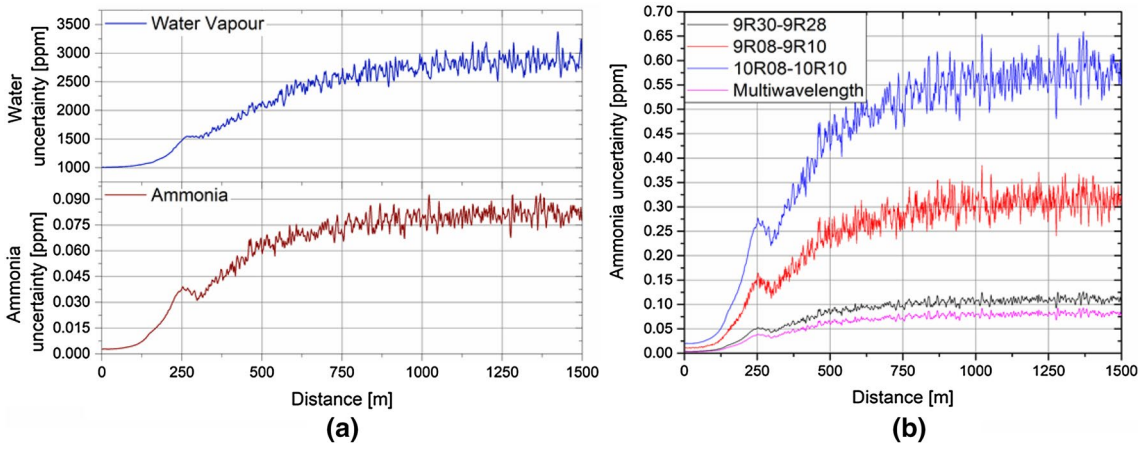

Fig. 7 Experimental uncertainties of water and ammonia measurements in function of distance (**a**) and ammonia uncertainties of DIAL couples and multiwavelength approach (**b**)

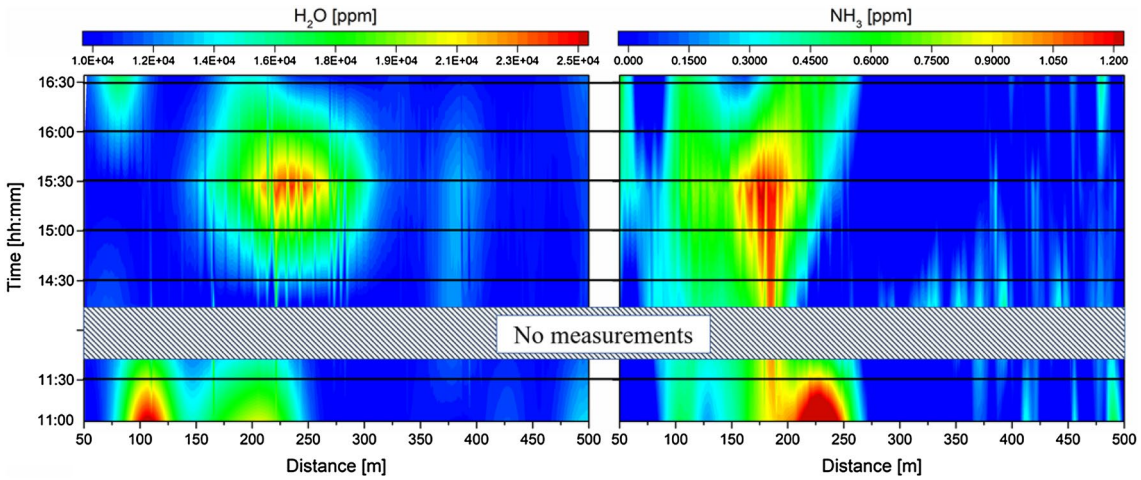

Fig. 8 Concentration map of water vapour and ammonia in function of distance and time

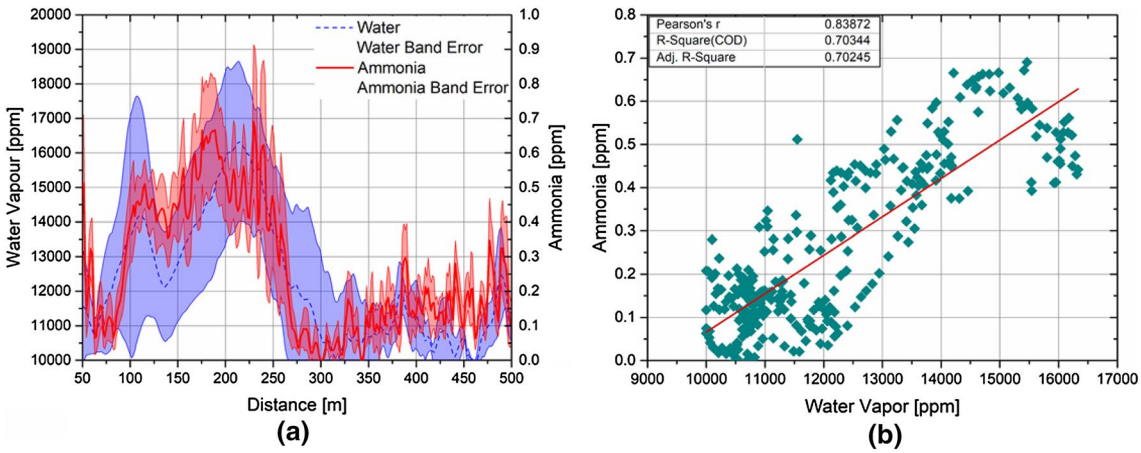

Fig. 9 Mean concentration and uncertainty band of water and ammonia along the measurement area (**a**) and the correlation between water vapour and ammonia concentration measurements (**b**)

100%, the minimum 34%, and the mean 58% [53]. Using a psychrometric chart, a mean value of 15,000 ppm of water vapour has been evaluated.

Water vapour map shows large increments in the region between 150 and 300 m, corresponding to the roundabout. An increase of water is expected over a high traffic area, since water vapour is a product combustion process. Water vapour also increases in the region between 75 and 125 m at 11:00 and 16:00. In this case, the increase of water vapour corresponds to the beginning and the end of the working time which led an increase of the traffic in the parking region. The ammonia map shows the concentration field obtained through the multiwavelength approach. The map shows a significant increase of ammonia in the same region of water vapour map in correspondence of area with a large traffic. The increase of ammonia over a high traffic region is expected [54–56]. The maximum value reached was lower than 1.2 ppm and the mean value in the traffic region was 1 ppm.

Figure 9a shows the average trend of water vapour and ammonia versus range, while Fig. 9b shows the correlation between these data. The correlation is quite strong ($R^2 = 0.7$). The increase of water vapour concentrations corresponds to an increase of ammonia and it implies that both chemical compounds are closely related to exhaust gas emissions from vehicles. A better fit is not reached because of several remarks to consider. At first, the water vapour and ammonia signals are not taken simultaneously, but there are several minutes between the measurements and natural variations which imply different instantaneous profiles. This is the reason why instantaneous data have

a lower correlation ($R^2 < 0.5$). Furthermore, the emission of water vapour is not linearly correlated to the ammonia one. Water vapour is a product of combustion, while ammonia is used in selective catalytic reduction (SCR) to reduce NOx emissions. Moreover, vehicles use different combustibles and different amount of ammonia in the SCR [54–56]. The last remark to consider is the possible production of water vapour and ammonia from other sources which are not correlated. All these issues worsen the water–ammonia fit.

3.5 Discussion

The use of a multiwavelength method for DIAL measurements may involve interesting improvements in the technique accuracy. The generalization of the multiwavelength method led to the possibility of using different wavelength couples. The uncertainty reduction achieved with this method has been calculated and shown previously. The uncertainty obtained is 25% less of the most accurate couple. However, the multiwavelength method requires caution when used. At first, a proper evaluation of extinction and backscattered coefficients influence should be done. A large error on one couple may involve an increase of the multiwavelength error major than some single couple, nullifying the aim of this approach. Uncertainties of couples should be evaluated, as well.

Another important issue must be considered. The use of a DIAL technique is based on the "instantaneous" measurement hypothesis. It means that the "on" and the "off" wavelengths should be acquired with a time difference small enough to assume that nothing has changed in the measurements area. This hypothesis is the reason why atmospheric turbulence is one of the major sources of error in the DIAL measurements. Several researchers solved the problem using two lasers: one for the "on" signal and one for the "off". This natural turbulence also affects the multiwavelength method, since the measured concentration profiles are not taken simultaneously. However, it is fundamental to separate the two different cases: the measurement of the instantaneous values and the measurement of the average values. In the first case, the measurement time must be lower than the turbulent constant time of the atmosphere. Thus, a system with multiple lasers is required, where each laser perform the measurement of one line, since the switching line is too low (the time delay between each line measurement should be lower than 100 μs). Contrariwise, the measurement of average values may not require multiple lasers, if the average value is statistically stable. It means that the average value during the measurement time can be considered constant. In this case, the approach used in this work can be used. In fact, averaging a lot of signals allows obtaining the average signal, which represents the average information at this wavelength.

The average value of gas concentrations in the atmosphere can be considered statistical steady only in some conditions, as a function of the weather and gas sources. Consider the following two examples: a roundabout crossed by one car every 1 min and a roundabout crossed continuously by several cars. Suppose that the DIAL measurement needs 2 min. In the first case, this DIAL apparatus cannot be used, since the emission of gas is related to a single event which happens with a low statistic and influence in significant ways the average values to measure. In this case, the fluctuations are of the same order of the measurement time. In the second case, there are several sources of chemicals with large frequency, to large to imagine the gas source like one continuous emission. In this case, the average values remain statistically constant, because the fluctuation due to one source of gas is balanced by the fluctuations of the other gas sources. In the second case, the DIAL apparatus with only one laser source can be used.

To verify that steadiness, it is possible to approach the problem with different techniques:

1. theoretical evaluation of the phenomenon;
2. numerical simulations;
3. experimental analysis.

The experimental analysis of the statistical steadiness of the phenomenon could be done by analysing how each line signal evolves during a time Δt. Now, divide the LIDAR signals into sub-groups, obtained during a time $\Delta t1$, $\Delta t2\ldots$ Δtn, where $\Delta t1 + \Delta t2 \cdots + \Delta tn = \Delta t$. If the average of each sub-group is statistically equal to each other, it is possible to affirm that the phenomenon is statistical steady in this time interval. This analysis should be performed with all the wavelengths used by the multiwavelength DIAL. In our case, the steadiness of the LIDAR signals has been proved.

In this work, the statistical steadiness has been tested and validated. The authors found that, between two following scan (3 min), the average variation of the signals was lower than 1%, while the mean relative standard deviation of the signal was larger than 15%. After three scans, this value becomes 4% and it reaches unacceptable values (> 15%) only after 20 min.

The use of a multiwavelength approach led to a decrease in the uncertainty of 25% (relative to the most accurate couple). The systematic error has been also evaluated and it remains much smaller (< 0.1%) than the ammonia measured in the atmosphere. These measurements of ammonia showed large values over the traffic area and the data have been correlated with the water vapour measurements. The correlation is high considering the phenomenon and all the

limits discussed before. The minimum concentration curves showed that the limit for ammonia is small if compared with the limit of breathable ammonia, 25 ppm for 8 h and 35 ppm for 15 min. Therefore, this system may be eligible to monitor area subjected to high risk of ammonia release (accidental or not).

4 Conclusions

In this work, the authors showed the multiwavelength approach in DIAL measurements, a technique based on the use of many "on" and "off" signals to obtain the concentration of one chemical compound. The aim of a multiwavelength approach is to improve the accuracy of the measurement. The analytical study of uncertainty propagation has been discussed. Then, they tested the method with the measurement of ammonia in a traffic area and they used the water vapour measurements to validate them.

The main difference with the Xiang work is about the line combinations, since this work extends the technique to a more generalised method. Furthermore, the multiwavelength equation when the complete DIAL equation is used has been obtained, highlighting the effect of extinction and backscattering coefficients.

The authors quantified the uncertainty of multiwavelength method through the uncertainty propagation theory and found that there are cases where the method is not recommended. In fact, a couple with large uncertainty may involve a multiwavelength uncertainty larger than some single couples. The propagation of the effect of extinction and backscattered coefficient has been evaluated, since it may disturb the measurements in significant ways.

The main limit of multiwavelength approach could be the measurement time, due to the switching line delay and the large number of lines to perform. This limit has been highlighted and discussed in the text, showing two possible cases: measurement of average and instantaneous (turbulent) values. In the first case, the device shown in this work can be used. Otherwise, a more complex multilaser-based apparatus should be built.

The measurements of ammonia and water vapour have been taken through our new DIAL system. It is an infrared CO_2-based apparatus able to perform measurement of several lines (more than 60). The system has also equatorial motors to perform areal measurements. Ammonia concentration profiles are according to the water vapour trends. There are mainly two areas where water and ammonia are present in large amounts. One is over the roundabout. In this area, the presence of ammonia and water vapour is always present, and it was expected, since the roundabout is trafficked the entire day. The other region is over the parking of the engineering departments, especially during the starting and finishing of the working time (11:00–11:30 and 16:00–16:30). A correlation between ammonia and water vapour has been found. The correlation degree is enough large, and it means that the water vapour and ammonia measured mainly due to emission from vehicles.

The capability of the system to read small values of ammonia in atmosphere confirms that the capability of this system is capable to monitor ammonia over large areas and provides a proper and fast response before that concentration of pollutants reaches a dangerous level.

References

1. J.H. Seinfeld, S.N. Pandis, *Atmospheric Chemistry and Physics—From Air Pollution to Climate Change* (Wiley, New York, 2016)
2. C.B. Field, V.R. Barros, D.J. Dokken, K.J. Mach, M.D. Mastrandrea, *Climate Change 2014—Impacts, Adaptation, and Vulnerability* (IPCC-Intergovernmental Panel on Climate Change, Geneva, 2014)
3. K.R. Smith, *Biofuels, Air Pollution, and Health: A Global Review* (Springer Science & Business Media, Berlin, 2013)
4. K. Zhang, S. Batterman, Air pollution and health risks due to vehicle traffic. Sci. Total Environ. **450–451**, 307–316 (2013)
5. L.B. Lave, E.P. Seskin, *Air Pollution and Human Health* (Earthscan, New York, 2011)
6. Environmental Pollution Centers, Air Pollution Diseases (2017) **(online)**. https://www.environmentalpollutioncenters.org/air
7. X.Q. Jiang, X.D. Mei, D. Feng, Air pollution and chronic airway diseases: what should people know and do?. J. Thorac. Dis. **8**(1), E31–E40 (2016)
8. T. Bourdrel, M.A. Bind, Y. Béjot, O. Morel, J.F. Argacha, Cardiovascular effects of air pollution. Arch. Cardiovasc. Dis. **110**(11), 634–642 (2017)
9. R.P. Pohanish, *Toxic and Hazardous Chemicals and Carcinogens* (Elsevier, Chennai, 2017)
10. J.C. Rippey, M.I. Stallwood, Nine cases of accidental exposure to dimethyl sulphate—a potential chemical weapon. Emerg. Med. J. **22**, 878–879 (2004)
11. A.J. Tomassoni, R.N. French, F.G. Walter, Toxic industrial chemicals and chemical weapons—exposure, identification and management by syndrome. Emerg. Med. Clin. N. Am. **33**, 13–36 (2015)
12. World Health Organization, Deliberate chemical release. (2017). http://www.who.int/environmental_health_emergencies/deliberate_events/chemical_release/en/. Accessed 18 Apr 2018 **(online)**
13. C. Ortolani, M. Vitale, The importance of local scale for assessing, monitoring and predicting of air quality in urban areas. Sustain. Cities Soc. **26**, 150–160 (2016)
14. G. Ottinger, E. Sarantschin, Exposing infrastructure: how activists and experts connect ambient air monitoring and environmental health. Environ. Sociol. **3**(2), 155–165 (2016)
15. T. Shah, J. Jawas, H. Mohd, K.A. Al Farisi, J.C. Banluta, Personal exposure monitoring of hazardous chemicals, in *Abu Dhabi International Petroleum Exhibition and Conference, Abu Dhabi* (2016)
16. V.A. Kovalev, W.E. Eichinger, *Elastic Lidar—Theory, Practice and Analysis Methods* (Wiley, Hoboken, 2004)
17. D.K. Killinger, A. Mooradian, *Optical and Laser Remote Sensing* (Springer, Berlin, 1983)
18. J.U. Eitel, B. Höfle, L.A. Vierling, A. Abellán, G.P. Asner, J.S. Deems, C.L. Glennie, P.C. Joerg, A.L. LeWinter, T.S. Magney, G.

Mandlburger, D.C. Morton, J. Müller, K.T. Vierling, Beyond 3-D: The new spectrum of lidar applications for earth and ecological sciences. Remote Sens. Environ. **186**, 372–392 (2016)
19. K. Koenig, B. Höfle, M. Hämmerle, T. Jarmer, B. Siegmann, H. Lilienthal, Comparative classification analysis of post-harvest growth detection from terrestrial LiDAR point clouds in precision agriculture. ISPRS J. Photogramm. Remote Sens. **104**, 112–125 (2015)
20. F. Duschek, L. Fellner, F. Gebert, K. Grünewald, A. Köhntopp, M. Kraus, P. Mahnke, C. Pargmann, H. Tomaso, A. Walter, Standoff detection and classification of bacteria by multispectral laser-induced fluorescence. Adv. Opt. Technol. **6**(2), 75–83 2017
21. P. Gaudio, M. Gelfusa, A. Murari, R. Pizzoferrato, M. Carestia, O. Cenciarelli, S. Parracino, G. Ludovici, J. Gabriele, V. Gabbarini, D. Di Giovanni, R. Rossi, J.-F. Ciparisse, C. Bellecci, A. Malizia, Application of optical techniques to detect chemical and biological agents. Defence S Tech. Bull. **10**(1), 1–13 (2017)
22. P. Weibring, H. Edner, S. Svanberg, G. Cecchi, L. Pantani, R. Ferrara, T. Caltabiano, Monitoring of volcanic sulphur dioxide emissions using differential absorption lidar (DIAL), differential optical absorption spectroscopy (DOAS), and correlation spectroscopy (COSPEC). Appl. Phys. B **67**(4), 419–426 (1998)
23. N. Cao, S. Li, T. Fukuchi, T. Fujii, R.L. Collins, Z. Wang, Z. Chen, Measurement of tropospheric O_3, SO_2 and aerosol from a volcanic emission event using new multi-wavelength differential-absorption lidar techniques. Appl. Phys. B **85**(1), 163–167 (2006)
24. C. Bellecci, M. Francucci, P. Gaudio, M. Gelfusa, S. Martellucci, M. Richetta, T. Lo Feudo, Application of a CO_2 dial system for infrared detection of forest fire and reduction of false alarm. Appl. Phys. B Lasers Opt. **87**(2), 373–378 (2007)
25. P. Gaudio, C. Bellecci, I. De Leo, M. Gelfusa, T. Lo Feudo, S. Martellucci, M. Richetta, Reduction of false alarms in forest fire surveillance using water vapour concentration measurements. Opt. Lasers Technol. **41**, 374–379 (2009)
26. C. Weitkamp, *Lidar—Range-Resolved Optical Remote Sensing of the Atmosphere* (Springer, Geesthacht, 2005)
27. R. Sa, L. Bu, Q. Wang, J. Zhou, Spectral characteristics of polluted gases and their detection by mid-infrared differential absorption lidar. Optik Int. J. Light Electron. Opt. **149**, 113–124 (2017)
28. S.M. Spuler, T. Weckwerth, K. Repasky, M. Hayman, A. Nehrir, Testing and validation of a micro-pulse, differential absorption lidar (DIAL) for measuring the spatial and temporal distribution of water vapor in the lower atmosphere, in *Light, Energy and the Environment, OSA Technnical Digest* (2016)
29. T.M. Weckwerth, K.J. Weber, Validation of a water vapor micropulse differential absorption lidar (DIAL). J. Atmos. Ocean. Technol. **33**, 2353–2372 (2016)
30. H. Kildal, R.L. Byer, Comparison of laser methods for the remote detection of atmospheric pollutants. Proc. IEEE **59**, 1644–1663 (1971)
31. R. Robinson, T. Gardiner, F. Innocenti, P. Woods, M. Coleman, Infrared differential absorption lidar (DIAL) measurements of hydrocarbon emissions. J. Environ. Monit. **13**(8), 2213–2220 (2011)
32. F. Innocenti, R. Robinson, T. Gardiner, A. Finlayson, A. Connor, Differential absorption lidar (DIAL) measurements of Landfill methane emissions. Remote Sens. **9**(9), 953 (2017)
33. S.M. Spuler, K.S. Repasky, B. Morley, D. Moen, M. Hayman, A.R. Nehrir, Field-deployable diode-laser-based differential absorption lidar (DIAL) for profiling water vapor. Atmos. Meas. Tech. **8**, 1073–1087 (2015)
34. I. Robinson, J.W. Jack, C.F. Rae, J.B. Moncrieff, Development of a laser for differential absorption lidar measurement of atmospheric carbon dioxide. Proc. SPIE **9246**, 92460U (2014)
35. S.I. Dolgii, A.A. Nevzorov, A.V. Nevrozov, O.A. Romanovskii, O.V. Kharchenko, Intercomparison of ozone vertical profile measurements by differential absorption lidar and IASI/MetOp satellite in the upper troposphere–lower stratosphere. Remote Sens., **9**(5), 447 2017
36. M.A. Sutton, D. Fowler, Introduction: fluxes and impacts of atmospheric ammonia on national, landscape and farm scales. Environ. Pollut. **119**(1), 7–8 (2002)
37. M.A. Sutton, J.W. Erisman, F. Dentener, D. Möller, Ammonia in the environment: from ancient times to the present. Environ. Pollut. **156**(3), 583–604 (2008)
38. S.N. Behera, M. Sharma, Investigating the potential role of ammonia in ion chemistry of fine particulate matter formation for an urban environment. Sci. Total Environ. **408**, 3569–3575 (2010)
39. K.M. Updyke, T.B. Nguyen, S.A. Nizkorodov, Formation of brown carbon via reactions of ammonia with secondary organic aerosols from biogenic and anthropogenic precursors. Atmos. Environ. **63**, 22–31 (2012)
40. A.F. Bouwman et al., A global high-resolution emission inventory for ammonia. Glob. Biogeochem. Cycl. **11**, 561–587 (1997)
41. N.T. Phan et al., Summer ammonia measurements in a densely populated Mediterranean city. Atmos. Chem. Phys. **12**, 7557–7575 (2012)
42. S. Wang, et al., Atmospheric ammonia and its impacts on regional air quality over the megacity of Shanghai, China. Sci. Rep. **5**, 15842 (2015)
43. O. Safety, H. Administration, Ammonia [Online]. https://www.osha.gov/dts/chemicalsampling/data/CH_218300.html. Accessed 18 Apr 2018
44. S. Bittman, J.R. Brook, A. Bleeker, T.W. Bruulsema, Air quality, health effects and management of ammonia emissions from fertilizers, in *Air Quality Management* (2013), pp. 261–277
45. C. Xiang, X. Ma, A. Liang, G. Han, W. Gong, F. Yan, Feasibility study of multi-wavelength differential absorption LIDAR for CO_2 monitoring. Atmosphere **7**(89), 1–17 (2016)
46. D.K. Killinger, N. Menyuk, Remote probing of the atmosphere using a CO_2 DIAL system. IEEE J. Quantum Electron. QE-17(9), 1917–1929 (1981)
47. R.W. Fenn, S.A. Clough, W.O. Gallery, R.E. Good, F.X. Kneizys, J.D. Mill, L.S. Rothman, E.P. Shettle, F.E. Volz, Chapter 18—Optical and Infrared Properties of the Atmosphere
48. R.A. McClatchey, A.P. D'Agati, Atmospheric transmission of laser radiation: computer code LASER. AFGL-TR-78-0029 (1978)
49. A. Ben-David, Backscattering measurements of atmospheric aerosols at CO_2 laser wavelengths: implications of aerosol spectral structure on differential-absorption lidar retrievals of molecular species. Appl. Opt. **38**(12), 2616–2624 (1999)
50. The HITRAN Database [Online]. http://hitran.org. Accessed 18 Apr 2018
51. T. Fujii, T. Fukuchi, *Laser Remote Sensing* (CRC Press, Boca Raton, 2005)
52. C. Bellecci, L. De Leo, P. Gaudio, T. Lo Feudo, S. Martellucci, M. Richetta, Water vapour emission in vegetable fuel: absorption cell measurements and detection limits of our CO_2 Dial system. Proc. SPIE **6367**, 63670I (2006)
53. Il Meteo [Online]. https://www.ilmeteo.it/portale/archivio-meteo/Roma/2017/Settembre/28. Accessed 18 Apr 2018
54. M. Elser, I. El-Haddad, M. Maasikmets, C. Bozzetti, R. Wolf, G. Ciarelli, J.G. Slowik, R. Ritcher, E. Teinemaa, C. Hüglin, U. Baltensperger, A.S. Prévot, High contributions of vehicular emissions 1 to ammonia in three European cities derived from mobile measurements. Atmos. Environ. 169, 36 (2017)
55. R. Suarez-Bertoa, C. Astorga, Isocyanic acid and ammonia in vehicle emissions. Transport. Res. Part D **49**, 259–270 (2016)
56. R. Suarez-Bertoa, A.A. Zardini, C. Astorga, Ammonia exhaust emissions from spark ignition vehicles over the New European Driving Cycle. Atmos. Environ. **97**, 43–53 (2014)